

Two critical temperatures conundrum in $\text{La}_{1.83}\text{Sr}_{0.17}\text{CuO}_4$

Abhisek Samanta¹, Itay Mangel², Amit Keren², Daniel P. Arovas³, Assa Auerbach²

¹ Department of Physics, The Ohio State University, Columbus OH 43210, USA,

² Physics Department, Technion, Haifa, Israel

³ Department of Physics, University of California at San Diego,
La Jolla, California 92093, USA

*Corresponding: assa@physics.technion.ac.il

May 3, 2024

Abstract

The in-plane and out-of-plane superconducting stiffness of $\text{La}_{1.83}\text{Sr}_{0.17}\text{CuO}_4$ rings appear to vanish at different transition temperatures, which contradicts thermodynamical expectation. In addition, we observe a surprisingly strong dependence of the out-of-plane stiffness transition on sample width. With evidence from Monte Carlo simulations, this effect is explained by very small ratio α of inter-plane over intra-plane Josephson couplings. For three dimensional rings of millimeter dimensions, a crossover from layered three dimensional to quasi one dimensional behavior occurs at temperatures near the thermodynamic transition temperature T_c , and the out-of-plane stiffness *appears* to vanish below T_c by a temperature shift of order $\alpha L_a/\xi^{\parallel}$, where L_a/ξ^{\parallel} is the sample's width over coherence length. Including the effects of layer-correlated disorder, the measured temperature shifts can be fit by a value of $\alpha = 4.1 \times 10^{-5}$, near T_c , which is significantly lower than its previously measured value near zero temperature.

1 Introduction

A homogeneous three-dimensional superconductor is expected to exhibit a single transition temperature T_c at which the order parameter, $\Delta(T)$, and all the superconducting stiffness components vanish [1, 2]. In this regard, recent measurements of the ab -plane (ρ^{\parallel}) and c -axis (ρ^{\perp}) stiffnesses of $\text{La}_{1.875}\text{Sr}_{0.125}\text{CuO}_4$ crystals by Kapon *et. al.* [3] have been puzzling. Counter to the expectation above, ρ^{\perp} was seen to vanish at T_c^{\perp} , which is about 0.64 K below the vanishing temperature T_c^{\parallel} of ρ^{\parallel} .

Disorder – Short range uncorrelated disorder is not expected to affect the critical behavior of a superconductor, by Harris's criterion [4]. On the other hand, the cuprates are known to be highly anisotropic layered superconductors. Layer-correlated disorder, (or a gradient in dopant concentration along the c axis) [5, 6], yields a distribution of ρ^{\parallel} and T_c^{\parallel} . Experimentally, such inhomogeneity is manifested by a high temperature tail of the measured ρ^{\parallel} above the average T_c^{\parallel} , while ρ^{\perp} vanishes at the lowest values of T_c^{\parallel} (see Appendix A). However, T_c^{\parallel} in Ref. [3] exhibited inhomogeneity broadening of ~ 0.1 K, which is significantly below the apparent difference in T_c 's.

Finite size effects – An alternative proposition is that finite sample dimensions play a role. Previous Monte-Carlo simulations [7, 8] of the 3dXY model found strong effects of sample dimensions on the temperature dependent stiffness coefficients. These effects are expected to be enhanced by high anisotropy.

This paper explores finite size effects experimentally and theoretically. We report systematic stiffness measurements near T_c for $\text{La}_{1.83}\text{Sr}_{0.17}\text{CuO}_4$ rings with widths L_a, L_c ranging between $L = 0.1$ to 1 millimeter. T_c^{\parallel} is found to be weakly dependent on L_c, L_a . In contrast, a significant reduction of T_c^{\perp} for decreasing width L_a is observed. This behavior is not expected for layer-correlated inhomogeneity. The relatively strong finite size effect demands theoretical explanation.

Phenomenologically, the monotonous relation between T_c and ρ^{\parallel} in cuprates [9], and the observed jump in ρ^{\parallel} at T_c in ultra-thin films [10], suggest that T_c is driven by superconducting phase fluctuations [11], and vortex unbinding [12]. Therefore we appeal to the three dimensional classical XY (3dXY) model (rather than BCS theory) to explain the stiffness temperature dependence toward T_c .

We applied a Monte-Carlo simulation with Wolff cluster updates on finite three dimensional lattices. The in-plane and intra-plane superconducting stiffness coefficients of the highly anisotropic 3dXY model appeared to vanish at different transition temperatures. The numerical simulations showed a strong dependence of the apparent inter-plane stiffness vanishing temperature T_c^{\perp} on the layers' finite width. This dependence exceeded the magnitude expected of critical fluctuations.

The numerical and experimental observations are understood as follows. Inter-layer mean field theory [13], predicts a thermodynamic transition temperature slightly above the two dimensional Berezinskii-Kosterlitz-Thouless [12] (BKT) transition at $T_{\text{BKT}} < T_c$. 3dXY critical behavior [1] is expected to be observed only very close to T_c . As temperature approaches T_c , the finite sample width L_a drives a crossover of ρ^{\perp} to the stiffness of a one dimensional XY (1dXY) chain [8]. This crossover results in an exponentially flat temperature dependence of $\rho^{\perp}(T, L_a)$ below T_c . For finite experimental or numerical resolution, such singular behavior always appears as vanishing of ρ^{\perp} at $T_c^{\perp}(L_a) < T_c$.

We compare our theoretical analysis to the experimental values $T_c^{\perp}(L_a)$, and use the fit to estimate of the anisotropy parameter of $\text{La}_{1.83}\text{Sr}_{0.17}\text{CuO}_4$ near its thermodynamic T_c .

2 Experiments

Measurements were carried out with a ‘stiffnessometer’ apparatus [14] which comprises of a long excitation coil piercing a superconducting ring. A bias current in the coil creates an Aharonov-Bohm (AB) vector potential \mathbf{A} which, by London’s equation, produces a persistent current that is measured by the induced (dia-)magnetization m^{α} along the coil axis α . One then measures m^{α} by moving a pickup loop relative to the ring and coil. The apparatus is shown in Fig. 1.

$\text{La}_{2-x}\text{Sr}_x\text{CuO}_4$ is known to grow in large single crystals allowing significant size reductions. Therefore, powder of different doping is prepared from stoichiometric ratios of 99.99% pure CuO , La_2O_3 , and SrCO_3 to make feed and seed rods. This powder is turned into a single crystal using an image furnace with four elliptic mirrors focusing 300 W halogen lamps. The growth was stabilised over 100 hr without any change of the lamp 59% power. Growth rate of 1.0 mm/h, down-ward translation of 0.15 mm/h, and rotation in opposite directions at 15 rpm were used. The emerging crystals looked like Fig. 1 of Ref. [15]. After the growth, the crystals were annealed in argon environment at $T = 850$ C for 120 hr to release internal stress. Finally, the crystals were oriented with a Laue camera, and cut into rings with a femtosecond laser cutter. For each doping two rings, labelled by a and c , were prepared with their coil axes parallel (a) and perpendicular (c) to the CuO_2 planes. The width and height of the rings was varied by the laser, or polished down to

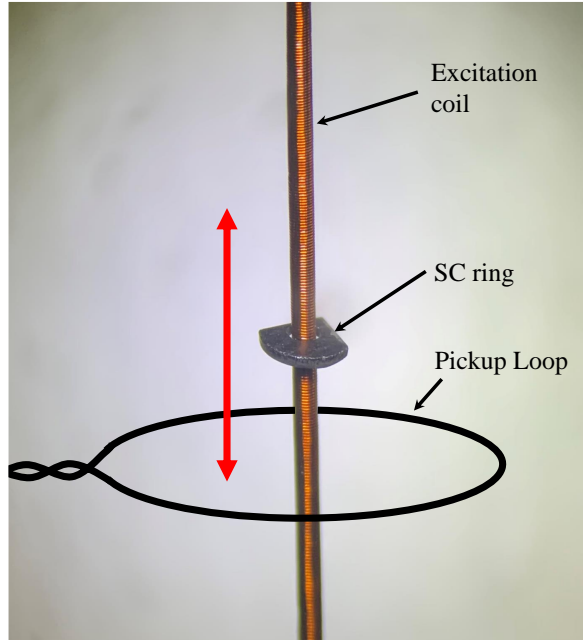


Figure 1: A superconducting ring cut in two directions, on the excitation coil. The red double arrow shows the moving direction of the schematic magnetization measuring pickup-loop, relative to both coil and ring.

the geometries shown in Fig. 2a,b.

For the a -ring, we varied mostly the narrowest (bottleneck) widths of the $a-b$ planes, L_a , whereas for the c -ring we varied both L_c and L_a (see Figs. 2a,b). Fig. 2(c) shows the narrowest bottleneck geometry of the a -ring. The requirement to: cut, measure, cut, measure, et cetera, the same pair of samples proved challenging. In most cases one of the samples broke during some step of the process. Only one pair of $\text{La}_{1.83}\text{Sr}_{0.17}\text{CuO}_4$ rings survived the reduction of L_a by factor of 10 between the initial and final cutting stages. The magnetization of this sample is depicted in Fig. 2.

When the transverse London penetration depth λ_c (λ_a) is smaller than the sample width L_c (L_a), the induced persistent current in the superconductor precisely cancels the AB flux of the coil. This results in a temperature independent induced magnetization m^a (m^c) at low temperatures.

As $T \rightarrow T_c$, the AB flux in the coil is under screened as $\lambda_\alpha(T) \geq L_\alpha$. In this temperature regime $m^\alpha(T)$ decreases rapidly and becomes linearly proportional to the in-plane stiffness components. As an example, for the geometry of a perfect ring

$$\begin{aligned}
 m^{a,c}(T) &= h \int_{r_{\text{in}}}^{r_{\text{out}}} dr \pi r^2 (\hat{r} \times \mathbf{j}_{\text{sc}}(r))^{a,c} \\
 &= -h(r_{\text{out}}^2 - r_{\text{in}}^2) \frac{\Phi}{4} \rho^{\perp,\parallel}(T) \quad .
 \end{aligned}
 \tag{1}$$

h , r_{in} , and r_{out} are the ring's height, and inner and outer radii, and Φ is the flux produced by the coil. For irregular rings extracting $\rho^\perp, \rho^\parallel$ from $m^\alpha(T)$ requires a full solution of Ginzburg-Landau and Biot-Savart equations [16]. However, here we do not require the magnitude of $\rho^\perp, \rho^\parallel$ but only their vanishing temperatures T_c^\perp and T_c^\parallel . These are experimentally determined by the vanishing of the corresponding magnetizations.

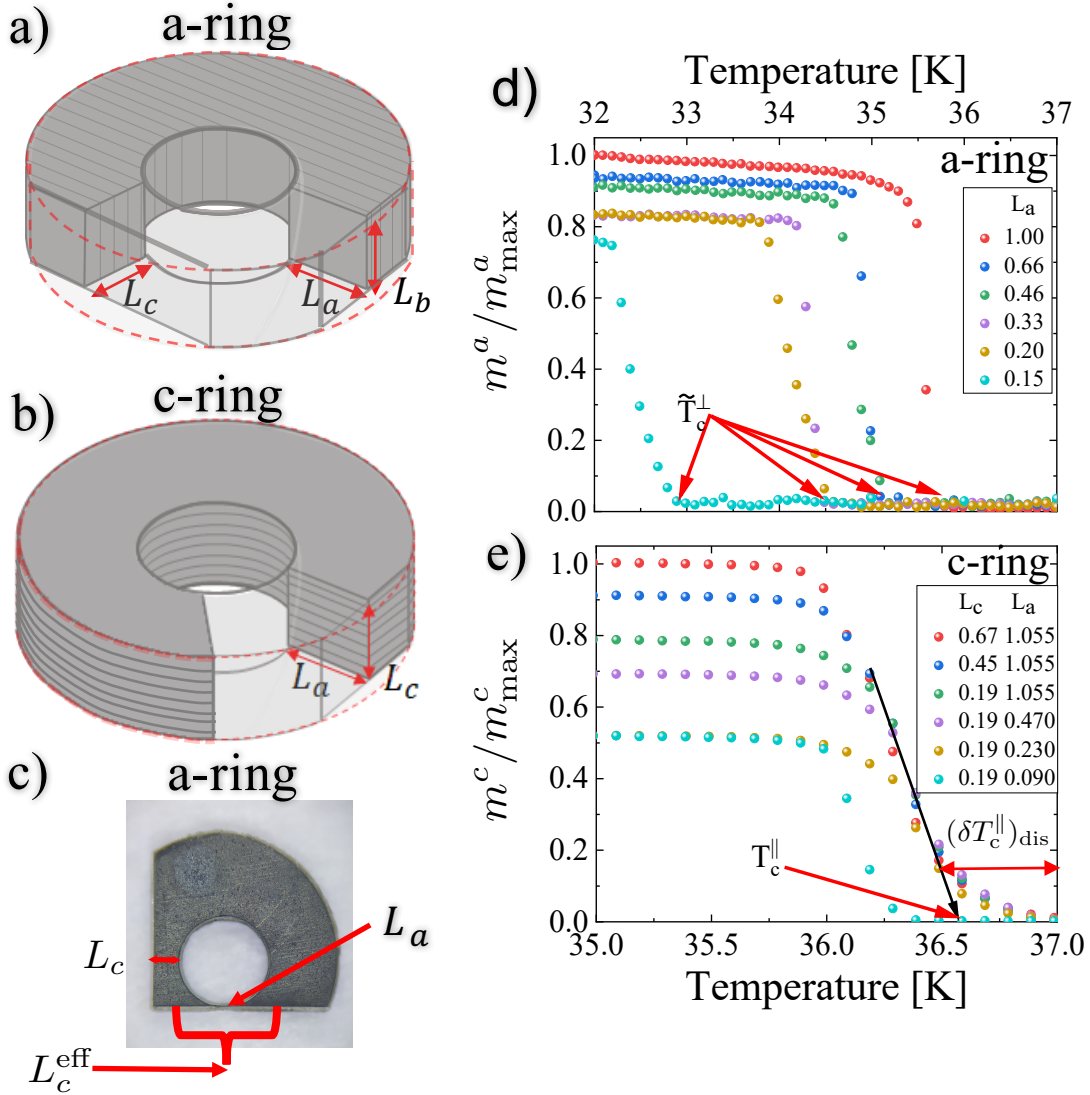


Figure 2: Experimental configuration and normalized magnetizations of $\text{La}_{1.83}\text{Sr}_{0.17}\text{CuO}_4$ rings for a fixed 1 mA current in the coil. (a) The interior of the *a*-ring. The CuO_2 planes are parallel to the ring's symmetry axis. This ring is sequentially polished to reduce the layers' width L_a in the bottleneck region. (b) The interior of the *c*-ring. The CuO_2 planes are perpendicular to the ring's symmetry axis. This ring is polished along two planes which varies both L_a and L_c . (c) Photograph of an *a*-ring with two cut planes. L_c^{eff} defines the effective aspect ratio in the bottleneck region. (d) Magnetization m^a of *a*-rings with variable L_a . The apparent stiffness vanishing temperatures are denoted by $\tilde{T}_c^\perp(L_a)$. (e) Magnetization m^c of *c*-rings. Except for the narrowest sample $L_a = 0.09$ (which is suspected of containing a traversing cut), the magnetizations near their transition are insensitive to L_a . The tail of width $(\delta T_c^\parallel)_{\text{dis}} \simeq 0.5$ K is assumed to reflect some layer-correlated disorder, which is a smaller effect than the finite size dependence of the *a*-rings' \tilde{T}_c^\perp . \tilde{T}_c^\parallel is averaged in-plane transition temperature (see Section 6 and Appendix A).

Figs. 2(d,e) depict the temperature-dependent relative magnetizations $m^\alpha(T, L_a)/m_{\text{max}}^\alpha$, for $\alpha = a, c$. m_{max}^α is the zero temperature magnetization of the largest ring. Fig. 2(d) shows a strong dependence of the *a*-ring's magnetization apparent vanishing temperature

\tilde{T}_c^\perp on the transverse width L_a . In contrast, the c -rings' magnetization in Fig. 2(e), exhibit insensitivity to the sample widths in the ranges $L_a \in [1.05, 0.23]$ and $L_c \in [0.67, 0.19]$. We note an exception of the $(L_a, L_c) = (0.09, 0.19)$ mm sample, which we believe to be damaged by a deep fracture during the cutting process.

We note that the c -ring magnetizations exhibit a high temperature tail of $\simeq 0.5$ K above the extrapolated transition at \tilde{T}_c^\parallel . This is attributed to layer-correlated inhomogeneity as discussed in the Introduction and Appendix A. This inhomogeneous broadening will be taken into account in fitting theory to the experimental data in Section 3.

3 Layered 3dXY model

As mentioned before, we model the phase fluctuations of $\text{La}_{1.83}\text{Sr}_{0.17}\text{CuO}_4$ near T_c by the classical 3dXY Hamiltonian on a tetragonal lattice,

$$H_{3dXY} = - \sum_i \sum_\gamma J_\gamma \cos(\varphi_{\mathbf{r}_i} - \varphi_{\mathbf{r}_i + \mathbf{a}_\gamma}) \quad , \quad (2)$$

where $\gamma \in \{a, b, c\}$ and where $J_a = J_b = J^\parallel$ and $J_c = J^\perp$ are the effective intra- and inter-plane Josephson couplings. The effective anisotropy parameter is defined as $\alpha = J^\perp / J^\parallel$. α will later be determined to fit experimental data near T_c . The two dimensional limit $\alpha = 0$ reduces to the two dimensional XY (2DXY) model, where by Mermin and Wagner theorem the superconducting order parameter $\Delta = \langle e^{i\varphi} \rangle$, and ρ^\perp vanish at all temperatures. Nevertheless, the in-plane stiffness is non-zero below $T_{\text{BKT}} \simeq 0.893J_a$.

For small but finite anisotropy $0 < \alpha \ll 1$, inter-layer mean field theory (IMFT) is very useful [13, 17–20]. It predicts $\Delta(T) > 0$ for $T < T_c$, where T_c is the three dimensional critical temperature. IMFT uses the exponential divergence of the BKT susceptibility above T_{BKT} to obtain,

$$\frac{T_c(\alpha) - T_{\text{BKT}}}{T_{\text{BKT}}} = \left(\frac{b}{|\ln(0.14\alpha)|} \right)^2 \quad . \quad (3)$$

Here, the (non universal) constant is taken to be $b = 2.725$ [21].

In the regime $[0, T_{\text{BKT}}]$, the order parameter magnitude $\Delta = |\langle e^{i\varphi} \rangle|$ decreases from unity as calculated by Hikami and Tsuneto [22],

$$\Delta^2(T)_{T < T_{\text{BKT}}} \simeq \exp\left(-\frac{T \log(1/\alpha)}{4\pi J_a}\right) \quad . \quad (4)$$

Over the crossover regime $T \in [T_{\text{BKT}}, T_c]$, the order parameter squared initially crosses over with an intermediate power law of $|T - T^*|^{0.46}$, where $T^* = T_{\text{BKT}} + \frac{1}{4}(T_c - T_{\text{BKT}})$ [19], above which it drops precipitously toward T_c as,

$$\Delta^2(T) = \Delta_{\text{BKT}}^2 t^{2\beta} \quad , \quad t \equiv \left(\frac{T_c - T}{T_c - T_{\text{BKT}}} \right) \quad , \quad (5)$$

where β crosses over from the mean field value $\frac{1}{2}$ to the 3dXY exponent 0.349, within a narrow three dimensional Ginzburg critical region of width $T_c / \log^4(\alpha)$ [13].

Fig. 3 depicts the smoothed ‘‘trapezoidal’’ temperature dependence of Δ^2 which differs from the BCS theory for the gap squared. We note that the spectral gaps observed by photoemission do not directly measure the thermodynamic order parameter. In the underdoped pseudogap phase [23], parts of the Fermi surface gap survives above T_c [24, 25]. A more direct measurement of Δ^2 near T_c would be the superconducting stiffness [1, 13], since

$$\rho_\gamma(T) \propto \Delta^{2-\eta\nu\beta^{-1}} \quad (6)$$

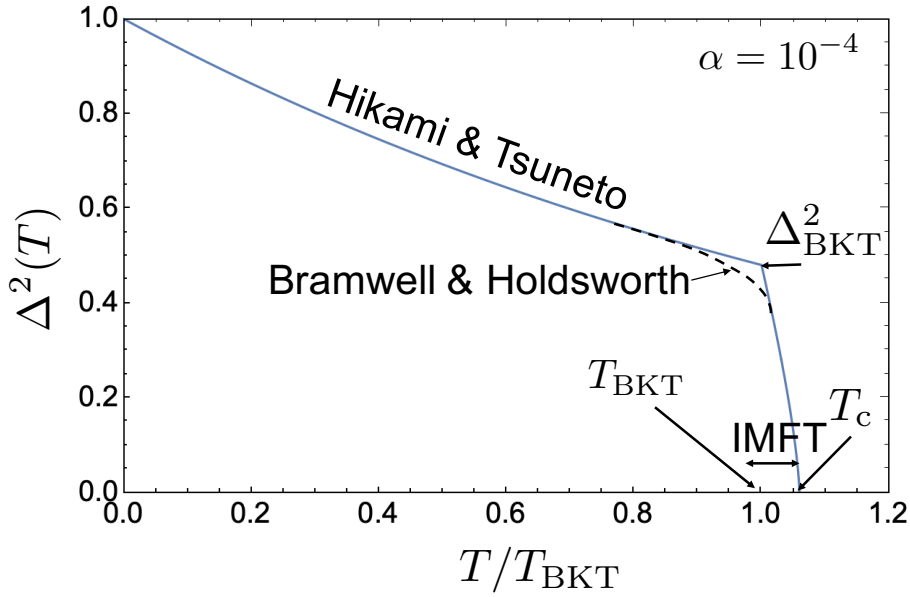


Figure 3: The order parameter squared as a function of temperature for the layered classical XY model, for anisotropy parameter $\alpha = 10^{-4}$. The graph patches the linear spinwave theory of Hikami and Tsuneto [22], the crossover (dashed line) power law of Bramwell and Holdsworth [19], and the three dimensional critical point which is obtained by Inter-plane Mean Field Theory (IMFT) of Eqs. (3), (4) and (5).

where η and ν are the critical correlation function power law and correlation length exponents respectively. For the 3dXY model $\eta\nu = 0.0255$ which is small and henceforth neglected.

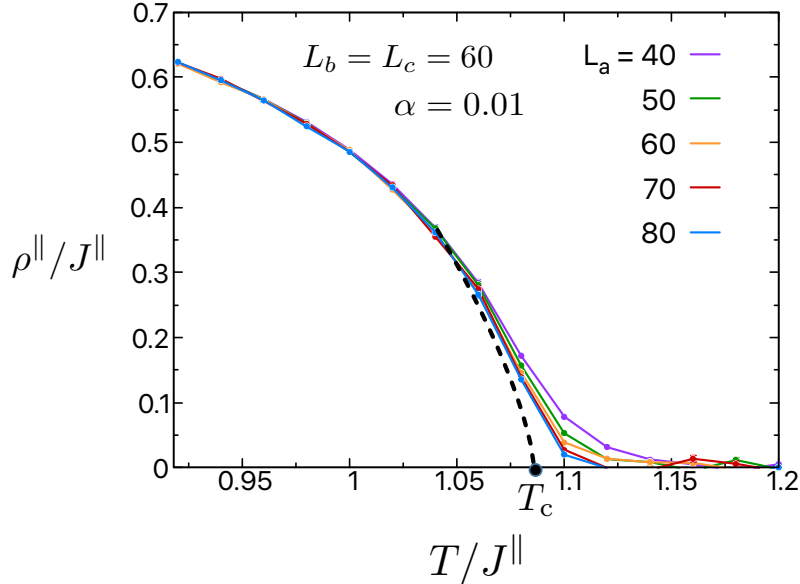


Figure 4: The intra-plane stiffness ρ^{\parallel} , plotted as a function of temperature T , for $\alpha = 0.01$ and for different L_a between 40 and 80, while L_b and L_c are kept fixed at 60. The error bars are smaller than the point sizes. The black dashed line shows the critical behavior near the thermodynamic transition temperature T_c , according to Eq. (6).

4 Monte Carlo simulations

The superfluid stiffness (*i.e.* helicity modulus) of Eq. 2 with $a_\gamma = 1$, is given by [7, 26]

$$\rho_\gamma = \frac{J_\gamma}{V} \left\langle \sum_{\langle ij \rangle} \cos(\varphi_{\mathbf{r}_i} - \varphi_{\mathbf{r}_j}) (r_i^\gamma - r_j^\gamma)^2 \right\rangle - \frac{J_\gamma^2}{VT} \left\langle \left(\sum_{\langle ij \rangle} \sin(\varphi_{\mathbf{r}_i} - \varphi_{\mathbf{r}_j}) (r_i^\gamma - r_j^\gamma) \right)^2 \right\rangle, \quad \gamma = a, b, c. \quad (7)$$

$V = L_a L_b L_c$. The first contribution measures the short range correlations, which are proportional to minus the energy along the bonds in the γ direction. The second contribution measures long range current fluctuations, which vanish at zero temperature, and reduce the stiffness at finite temperatures.

We compute Eq. (7) by a Monte Carlo (MC) simulation of H_{3dXY} with the Wolff cluster updates algorithm [27], see Appendix D for details. We choose $L_c = L_b = 60$, and vary the width in the range $L_a \in \{40, 50, \dots, 80\}$ using the anisotropy parameters in the range $\alpha = 0.01 - 0.02$. The minimal accessible anisotropy parameter is determined by the maximal lattice size.

In Fig. 4, we plot the intra-plane stiffness ρ^\parallel as a function of temperature T , and width L_a . The anisotropy parameter is fixed at $\alpha = 0.01$. $T_c \simeq 1.086$. The expected thermodynamic critical behavior, Eq. (6), is depicted by a dashed line in Fig. 4. For the disorder-free model, the tail above T_c indicates that the in-plane correlation length exceeds L_a . Thus, a larger L_a reduces the width of the tail. For millimeter scale superconducting rings, this tail should be unobservably small.

In Fig. 5, the MC data for $\rho^\perp(T)$ are shown as points. Given a numerical resolution threshold ε , $\rho^\perp(T)$ appears to vanish at transition temperatures \tilde{T}_c^\perp which depend on ε and the width L_a . The solid lines and the inset describe a fit of the MC data to analytic formulas derived in the following Section.

5 Crossover to one dimensional Josephson array

The *apparent* premature vanishing of ρ^\perp in a finite size sample of an approximately unit aspect ratio, is due to its crossover to a quasi one-dimensional behavior as $T \rightarrow T_c$. The stiffness of a one dimensional (1d) classical XY chain with inter-site coupling J_{1d} , lattice constant a and chain length L is well known,

$$\rho_{1d}(T, L) = TLZ_2/Z_0 \quad (8)$$

$$Z_{2p} = \sum_{n=-\infty}^{\infty} \left(\frac{I_n(J_{1d}/T)}{I_0(J_{1d}/T)} \right)^{L/a} n^{2p},$$

where I_n are modified Bessel functions and $p = 0, 1$. Luttinger liquid (LL) theory [8, 28], which applies at $L \gg a$, yields an analytic result where ρ_{1d} depends on the dimensionless variable $x \equiv LT/(J_{1d}a)$ as,

$$\rho_{LL}(J_{1d}, x) = J_{1d} a \left(1 - \frac{\pi^2}{x} \frac{\vartheta_3''(0, e^{-2\pi^2/x})}{\vartheta_3(0, e^{-2\pi^2/x})} \right) \quad (9)$$

$$\simeq J_{1d} a \begin{cases} 1 & (x \leq 2) \\ 20 \exp(-0.472 x) & (x \geq 10) \end{cases},$$

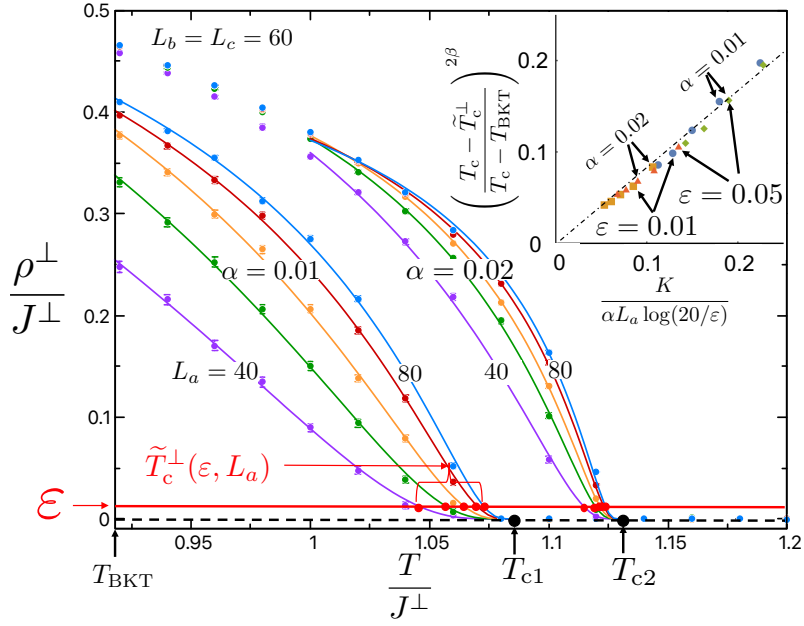


Figure 5: MC evaluations of ρ^\perp for the clean 3dXY model Eq. (2), a function of temperature for a range of sample widths $L_a \in \{40, 50, \dots, 80\}$, and anisotropy parameters α . The thermodynamic critical temperatures are evaluated as $T_{c1} = 1.086J_a$ and $T_{c2} = 1.13J_a$ for $\alpha = 0.01$ and 0.02 , respectively. Solid lines are best fits to Eq. (12). ε is arbitrarily chosen as the numerical resolution which defines the apparent transition temperatures \tilde{T}_c^\perp by Eq. (14). Inset: Verification of Eq. (15) by collapse of all the temperature shifts for various L_a, ε, α obtained from the main graphs.

where $\vartheta_3(z, q) = 1 + 2 \sum_{n=1}^{\infty} q^{n^2} \cos(2nz)$, and prime denotes differentiation with respect to z . Comparison between Eqs. (8) and (9) is shown in Appendix B.

Now we return to the c -axis stiffness ρ^\perp of the layered model (2), which can be described as a chain of Josephson junctions along the c -axis with inter-grain coupling,

$$J_{\text{eff}}(T) = \frac{L_a L_b}{(\xi^\parallel)^2} \times J^\perp \Delta^2(T), \quad (10)$$

Toward T_c , $\Delta^2(T)$ vanishes as $t^{2\beta}$ by Eq. (5). Substituting $J_{1d} = J_{\text{eff}}(T)$ we expect the asymptotic behavior of Eq. (9) to be realized after replacing

$$x \rightarrow \frac{L_c T}{J_{\text{eff}}(T) \xi^\perp}. \quad (11)$$

Thus for $t \ll 1$, $x \gg 1$ and

$$\rho^\perp(T) \approx 20 \rho^\perp(T_{\text{BKT}}) \exp\left(-\frac{K}{\alpha L_a} t^{-2\beta}\right), \quad (12)$$

$$K \simeq \frac{0.472 r T_c (\xi^\parallel)^2}{J_a \Delta_{\text{BKT}}^2 \xi^\perp}. \quad (13)$$

For any experimental resolution ε , an apparent vanishing temperature $\tilde{T}_c^\perp(\varepsilon)$ is defined by the threshold condition,

$$\frac{\rho^\perp(\tilde{T}_c^\perp)}{\rho^\perp(T_{\text{BKT}})} = \varepsilon. \quad (14)$$

By Eq. (12), the apparent width dependent transition temperature is,

$$T_c - \tilde{T}_c^\perp = (T_c - T_{\text{BKT}}) \left(\frac{K}{\alpha L_a \log(20/\varepsilon)} \right)^{1/2\beta} \quad (15)$$

The most important consequence of the quasi one-dimensional behavior, is that the temperature shifts are proportional to $(\alpha L_a)^{-1/2\beta}$. This is a much larger shift than expected from critical fluctuations, which are of order $(\alpha L_a^2)^{-1}$.

In the inset of Fig. 5 we verify the validity of Eq. (15) by collapsing of all the temperature shifts onto a straight line. The slope of this line differs only by 20% from unity, which we attribute to the choice of the (non-universal) constants in the asymptotic expression of Eq. (9).

6 Comparison of Theory to Experiments

In comparing Eq. 15 to the MC results, we have used the 3dXY critical exponent $\beta = 0.349$.

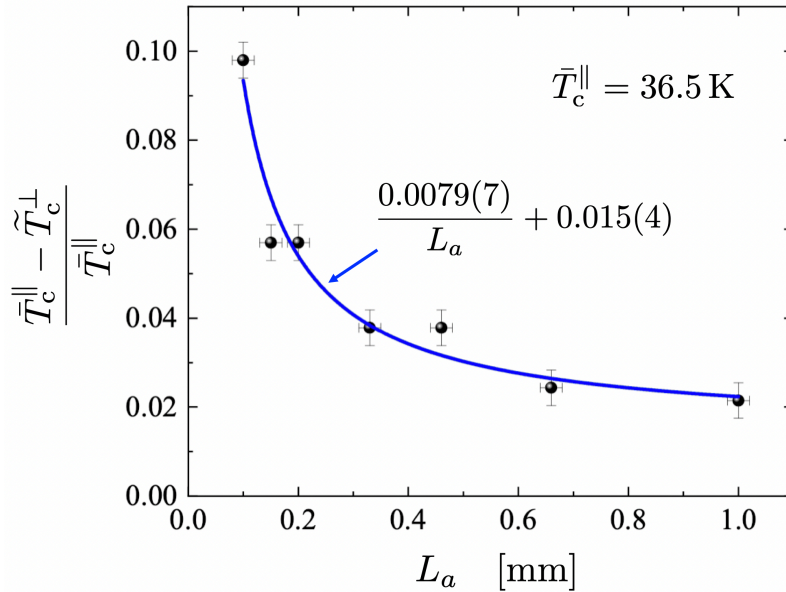


Figure 6: Comparison of experimental results for $\text{La}_{1.83}\text{Sr}_{0.17}\text{CuO}_4$ rings of Fig. 2 and theoretical prediction of Eqs. (15) and (19). Crosses: The apparent c -axis transition temperature shifts \tilde{T}_c^\perp of the a -rings, as determined in Fig. 2(d). L_a are the bottleneck widths of the ab planes. Line: the least square fit using $\alpha^{\text{fit}} = 4.1 \times 10^{-5}$. The offset of the reduced temperature 0.015(4) agrees with the estimated layer-correlated disorder (see text). We use the mean field exponent $\beta = \frac{1}{2}$, due to the narrow Ginzburg critical regime near T_c .

For the experimental $\text{La}_{1.83}\text{Sr}_{0.17}\text{CuO}_4$ crystals, the millimeter width corresponds to $\sim 10^5$ effective lattice constants, and the anisotropy parameter will turn out to be $\alpha < 10^{-4}$, which yields an unobservable narrow Ginzburg critical region. Hence we shall fit the Eq. 15 with the mean field exponent $\beta = 0.5$.

The a -ring is sequentially cut such that the induced current is governed by the bottleneck region. There, the induced current flows along the c axis over an effective length

of $L_c^{\text{eff}} = 2$ mm. The transverse dimension $L_b = 0.46$ mm yields $r = 4.34$. The width is varied in the range $L_a \in [0.1, 1]$ mm. We estimate the experimental resolution at $\varepsilon = 10^{-2}$. (High accuracy of ε is not essential, since \tilde{T}_c^\perp depends on it logarithmically).

At zero temperature the coherence lengths have been determined experimentally [29] to be $\xi^\parallel(0) \simeq 3$ nm and $\xi^\perp(0) \simeq 1.3$ nm. The in-plane lattice constant for the effective 3dXY model is the coherence length estimated at T_{BKT} to be $\xi^\parallel(T_{\text{BKT}}) = \xi^\parallel(0)/\Delta_{\text{BKT}}$. Due to the incoherent single-electron tunneling between the layers, we assume that the Cooper pair size in the c direction remains confined to a single plane $\xi^\perp(T_{\text{BKT}}) \simeq \xi^\perp(0)$.

In Fig. 6, the apparent c -axis transition temperatures $\tilde{T}_c^\perp(L_a)$ are plotted. The data is somewhat noisy, presumably because of the introduction of deep cuts during the ring's cutting process, which are eliminated by subsequent cuts. The two-parameter fit function is plotted,

$$\frac{\bar{T}_c^\parallel - \tilde{T}_c^\perp}{\bar{T}_c^\parallel} = \frac{A}{L_a[\text{mm}]} + (\delta t)_{\text{dis}} \quad (16)$$

with $A = 0.0079$ and $(\delta t)_{\text{dis}} = 0.015(4)$. The dimensionless temperature shift $(\delta t)_{\text{dis}}$ is understood as the effect of layer-correlated inhomogeneity (see Appendix A). We use the high temperature tail of magnitude $(\delta T_c^\parallel)_{\text{dis}} \simeq 0.5$ K, which is depicted in Fig. 2(e). Subtracting $(\delta T_c^\parallel)_{\text{dis}}$ from $\bar{T}_c^\parallel = 36.5$ K yields a bound for \tilde{T}_c^\perp for wide samples,

$$\lim_{L_a \rightarrow \infty} \tilde{T}_c^\perp = \bar{T}_c^\parallel - (\delta T_c^\parallel)_{\text{dis}} = 36 \text{ K}. \quad (17)$$

The estimated layer-correlated disorder shift is consistent with the fit in Fig. 6,

$$(\delta t)_{\text{dis}} \equiv \frac{(\delta T_c^\parallel)_{\text{dis}}}{\bar{T}_c^\parallel} \in 0.015(4). \quad (18)$$

Using Eqs. (3), (4), (13) and (15), and the parameters listed above we obtain

$$A = \Delta T_c(\alpha) \frac{0.472 \times 10^{-6} r T_c (\xi^\parallel)^2}{\alpha \Delta_{\text{BKT}}^4(\alpha) \xi^\perp \log(20/\varepsilon)} = 0.0079 \quad (19)$$

which can be fit by the anisotropy parameter,

$$\alpha^{\text{fit}}(T \simeq T_c) = 4.1 \times 10^{-5} \quad (20)$$

7 Discussion and Summary

The experimental conundrum, which was first noted in Ref. [3], was that stiffness measurements of a -rings and c -rings, cut out from same cuprate crystal, exhibited different transition temperatures. In this paper, we have shown that this difference cannot be fully explained by layer-correlated disorder, since it varies consistently with the layer's width, which is not coupled to the distribution of layer-correlated disorder.

With the help of Monte-Carlo simulations, inter-layer mean field theory, we have identified a narrow regime below the bulk transition temperature T_c where the inter-layer stiffness of finite size samples crosses over to an effective one dimensional Josephson array behavior. As a result, we resolve the conundrum, and explain the Monte-Carlo data, as a width-dependent, *apparent* reduction of the c -axis T_c . The visibility of the effect depends on the smallness of the anisotropy parameter α .

We note that α^{fit} parametrizes the effective Hamiltonian near T_c . We compare it to the zero temperature anisotropy parameter reported for optimally doped $\text{La}_{2-x}\text{Sr}_x\text{CuO}_4$ (for $\text{Sr}_{0.15}$) in Ref. [30],

$$\alpha^\lambda(T=0) = \left(\frac{\lambda_c}{\lambda_a}\right)^{-2} = 4.6 \times 10^{-3}. \quad (21)$$

The difference in anisotropy can be attributed to the reduction of inter-plane coherence due to thermally excited nodal quasiparticles of the d -wave superconductor and the effects of inter-planar vortex rings above the two dimensional T_{BKT} .

Analog in ^4He – We have seen that $\alpha \ll 1$ can be mapped onto an isotropic model on samples with large aspect ratio. A similar “premature” vanishing of ρ^\perp has been observed on a quasi-one dimensional brick, *i.e.* $L_a \ll L_c$ [7]. This result was used to explain the experimental disappearance of superfluid density of ^4He embedded in quasi one-dimensional nanopores [31,32]. Here we explain the *apparent* reduction of $\tilde{T}_c(L_a)$, not as a true thermodynamic transition but rather as a consequence of an essential singularity decay of ρ^\perp toward the thermodynamic T_c .

In general, layered superconductors with very high anisotropy are expected to exhibit such apparent differences between transition temperatures of in-plane and out of plane persistent currents. For example, an emergent anisotropy of layered superconductors has been an important consequence of certain pair density wave (PDW) ordering [33]. We propose that the dependence of inter-layer stiffness transition temperatures on sample width could help characterize the emergent anisotropy parameter of that interesting PDW phase.

8 Acknowledgements

A.S. and I.M. contributed equally to this work. We thank Erez Berg, Snir Gazit, Dror Orgad, and Daniel Podolsky for beneficial discussions. A.A. acknowledges the Israel Science Foundation (ISF) Grant No. 2081/20. A.K. acknowledges the ISF Grant. No. 1251/19 and 3875/21. This work was performed in part at the Aspen Center for Physics, which is supported by National Science Foundation grant PHY-2210452, and at the Kavli Institute for Theoretical Physics, supported by Grant Nos. NSF PHY-1748958, NSF PHY-1748958 and NSF PHY-2309135.

A Planar correlated disorder

Refs. [5,6] have considered the layered XY model where the ab planes exhibit a variable z -dependent stiffness $\rho^\parallel(z)$ for $z \in [0, L_c]$. We can see the effects of bounded correlated disorder on superconductors with a variation of $\rho^\parallel(z)$ along the c -axis. In each segment, the stiffness temperature dependence has a different T_c ,

$$\rho^\parallel(T) = \rho^\parallel(0) \left| \frac{T - T_c^\parallel(z)}{\bar{T}_c^\parallel} \right|^{2\beta - \eta\nu} \quad (22)$$

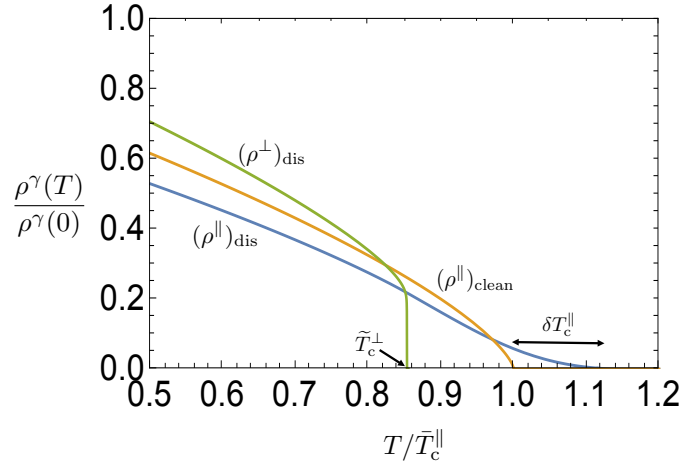


Figure 7: Effects of planar-correlated disordered, modelled by c -axis dependent in-plane stiffness $\rho^\parallel(z)$, with an average transition temperature \bar{T}_c^\parallel and a width of transition temperatures $(\delta T_c^\parallel)_{\text{dis}} = 0.1\bar{T}_c^\parallel$. Orange line: The clean system with a three dimensional critical behavior. Blue line: the global ρ^\parallel showing a disorder induced high temperature tail above \bar{T}_c^\parallel . Green line: the global ρ_\perp^{dis} , which is dominated by the weakest interplane stiffnesses, and vanishes below T_c^\parallel .

where $T_c^\parallel(z) \propto \rho^\parallel(z, 0)$ is the local transition temperature whose average is defined as \bar{T}_c^\parallel and maximal variation is $(\delta T_c^\parallel)_{\text{dis}}$. The global ab -stiffness is given by the integral

$$\rho^\parallel = \rho^\parallel(0) \int_0^{L_c} \frac{dz}{L_c} \left| \frac{T - T_c^\parallel(z)}{\bar{T}_c^\parallel} \right|^{2\beta - \eta\mu}, \quad (23)$$

which smears the average critical temperature \bar{T}_c^\parallel by a high temperature tail at $T \in [\bar{T}_c^\parallel, \bar{T}_c^\parallel + (\delta T_c^\parallel)_{\text{dis}}]$.

In contrast, the c -axis stiffness $\rho^\perp(z)/\rho^\perp(0)$ is proportional to the local order parameter squared $\Delta(z) \propto |T - T_c(z)|^\beta$. The global c -axis stiffness is the harmonic average given by,

$$\rho^\perp = \rho^\perp(0) \left(\int_0^{L_c} \frac{dz}{L_c} \frac{(\bar{T}_c^\parallel)^{2\beta}}{|T - T_c^\parallel(z)|^{2\beta}} \right)^{-1}. \quad (24)$$

The weakest segment, with the lowest $\rho^\perp(z)$, dominates the integral. The temperatures where the order parameter of this segment vanishes is

$$\tilde{T}_c^\perp \leq \bar{T}_c^\parallel - (\delta T_c^\parallel)_{\text{dis}}, \quad (25)$$

above which the global $\rho^\perp(T)$ disappears. The effect of bounded layer-correlated disorder is demonstrated in Fig. 7.

B Asymptotic behavior of stiffness of a one dimensional XY chain

In Fig. 8 we depict the exact result of the stiffness of the one dimensional XY chain as given by Eq. (7) of the main text. At large L/a the graphs show convergence to the

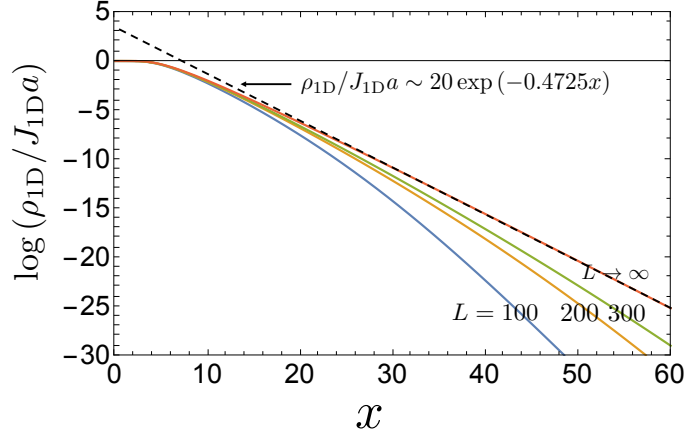


Figure 8: Stiffness as a function of scaled variable $x = LT/(J_{1d}a)$ in the one dimensional XY model for different lengths L as given by the exact result of Eq. (7), and asymptotically at $L \rightarrow \infty$ by Eq. (8) of the main text.

analytic Luttinger-Liquid form [8, 28], which at large x is given by Eq. (8) of the main text.

C Estimation of finite size shift in T_c

Fine size scaling produce unobservably small finite size shifts of T_c for millimeter size samples, as shown by the following. The correlation lengths above T_{BKT} diverge as

$$\xi^{\parallel}(t) \simeq \frac{1}{\sqrt{\alpha}} \xi_a^{(0)} t^{-\nu} \quad , \quad \xi^{\perp}(t) \simeq \xi_c^{(0)} t^{-\nu} \quad (26)$$

where we use the Ginzburg-Landau definition of correlation lengths, $\xi_{\gamma}^{-1} \propto \sqrt{\rho_{\gamma}}$, to obtain the factor of $\sqrt{\alpha}$ between the divergent correlation length.

For Eq. (2) with sample dimensions $L_{\gamma}, \gamma = a, b, c$ the stiffness components near T_c vanish as [34],

$$\frac{\rho_c}{\rho_c(T_{\text{BKT}})} = t^{\nu} \Phi[x_a] \quad , \quad x_a = \xi_a(t)/L_a. \quad (27)$$

where $\Phi(x)$ is differentiable function with a finite value at $x = 0$. We expand Φ to linear order in ξ_a and set $\rho^{\perp} \rightarrow 0$ to obtain,

$$0 = \Phi_0 + \partial_{x_a} \Phi \times \left(\frac{t^{-\nu} \xi_a^{(0)}}{\sqrt{\alpha} L_a} \right) + \mathcal{O}(x_a^2) \quad (28)$$

which is solved by a positive shift of T_c by the amount

$$\delta t \simeq - \frac{\Phi_0}{\partial_a \Phi_{\gamma}} \left(\frac{\sqrt{\alpha} L_a}{\xi_a^{(0)}} \right)^{-1/\nu}. \quad (29)$$

For the experimental $\text{La}_{1.83}\text{Sr}_{0.17}\text{CuO}_4$ rings, taking $\alpha = 10^{-5}$, $L_a/\xi_a^{(0)} \sim 10^6$, yields $|\delta t| \leq 10^{-4}$, which is much below experimental temperature resolution.

D Details of the Monte-Carlo simulations using cluster algorithm

The superfluid stiffness or the helicity modulus (with $a_\gamma = 1$) for the classical Hamiltonian of Eq. (2) is given by Eq. (7) [7, 26, 35].

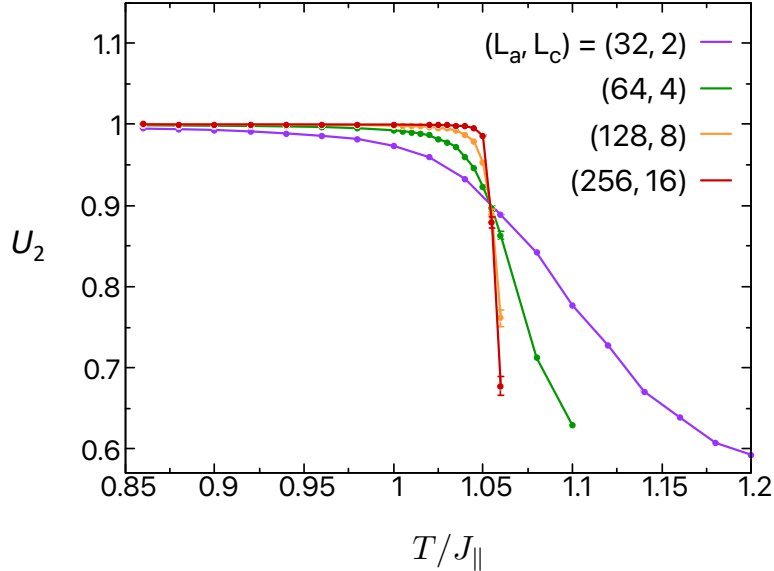


Figure 9: Binder cumulant U_2 plotted as a function of temperature T , for anisotropy $\alpha = 0.005$ and for different sizes with a fixed aspect ratio $L_a/L_c = 16$ and $L_b = L_a$.

In the Wolff-cluster algorithm [27], we assume the XY spins \mathbf{S} to be the unit vectors in \mathbb{R}^3 . In every Monte-Carlo (MC) step, we first choose a random site $\mathbf{r} \in \mathbb{R}^3$ and a random direction $\mathbf{d} \in S_2$, and consider a reflection of the spin on that site about the hyperplane orthogonal to \mathbf{d} . Note that this is equivalent to the spin-flipping operation in Ising model. We then travel to all neighboring sites (\mathbf{r}') of \mathbf{r} , and check if the bond $\langle \mathbf{r}\mathbf{r}' \rangle$ is activated with a probability

$$P_\gamma(\mathbf{r}, \mathbf{r}') = 1 - \exp\left(\min[0, 2J_\gamma\beta(\mathbf{d} \cdot \mathbf{S}_\mathbf{r})(\mathbf{d} \cdot \mathbf{S}_{\mathbf{r}'})]\right), \quad (30)$$

where β is the inverse temperature. If this satisfies, we mark \mathbf{r}' and include it to a cluster \mathcal{C} of “flipped” spins. We iteratively continue this process for all unmarked neighboring sites of \mathbf{r}' and grow the cluster size until all the neighbors turn out to be marked. We use such 10^6 number of MC steps for thermalization, followed by another 10^7 number of MC steps for measurement of different observables, such as the helicity modulus and the binder cumulant. We estimate the errors of different observables by using a standard Jackknife analysis of the MC data.

In Fig. 3 of the main text, we have presented the inter-plane superfluid stiffness ρ^\perp for different system sizes of $L_a \in [60 - 80]$, $L_b = L_c = 60$, near the transition.

Next we calculate the Binder cumulant, defined in terms of the higher powers of magnetization m as following [36]

$$U_2 = \frac{3}{2} \left(1 - \frac{1}{3} \frac{\langle m^4 \rangle}{\langle m^2 \rangle^2} \right), \quad (31)$$

and we use it to extract the value of critical temperatures accurately. As an example, in Fig. 9, we present U_2 as a function of T , for an anisotropy parameter $\alpha = 0.005$ and for

different system sizes with a fixed aspect ratio $L_a = L_b$ and $L_a/L_c = 16$. In the ordered phase when all the spins are aligned it takes a value 1, while in the disordered phase it vanishes and takes an intermediate value between 0 and 1 at the critical point. Therefore, by tracking the crossing between different system sizes, we find a critical temperature $T_c \sim 1.05$ for these parameters. using a similar analysis, we obtain T_c for other anisotropy parameters also, discussed in the main text.

References

- [1] M. E. Fisher, M. N. Barber and D. Jasnow, *Helicity Modulus, Superfluidity, and Scaling in Isotropic Systems*, Phys. Rev. A **8**, 1111 (1973), doi:10.1103/PhysRevA.8.1111.
- [2] M. Hasenbusch, *Monte Carlo study of an improved clock model in three dimensions*, Phys. Rev. B **100**, 224517 (2019), doi:10.1103/PhysRevB.100.224517.
- [3] I. Kapon, Z. Salman, I. Mangel, T. Prokscha, N. Gavish and A. Keren, *Phase transition in the cuprates from a magnetic-field-free stiffness meter viewpoint*, Nat. Comm. **10**(1), 2463 (2019), doi:10.1038/s41467-019-10480-x.
- [4] A. B. Harris, *Effect of random defects on the critical behaviour of Ising models*, Jour. Phys. C: Sol. State Phys. **7**(9), 1671 (1974).
- [5] P. Mohan, P. M. Goldbart, R. Narayanan, J. Toner and T. Vojta, *Anomalous intermediate phase in randomly layered superfluids, superconductors, and planar magnets*, Phys. Rev. Lett. **105**(8), 085301 (2010).
- [6] D. Pekker, G. Refael and E. Demler, *Finding the Elusive Sliding Phase in the Superfluid-Normal Phase Transition Smeared by c-Axis Disorder*, Phys. Rev. Lett. **105**, 085302 (2010), doi:10.1103/PhysRevLett.105.085302.
- [7] A. Kotani, K. Yamashita and D. S. Hirashima, *Superfluid density in quasi-one-dimensional systems*, Phys. Rev. B **83**, 174515 (2011), doi:10.1103/PhysRevB.83.174515.
- [8] D. S. Hirashima, *Helicity modulus of the quasi-one-dimensional XY model: Protection by an energy barrier*, Phys. Rev. B **102**(10), 104506 (2020).
- [9] Y. J. Uemura, G. M. Luke, B. J. Sternlieb, J. H. Brewer, J. F. Carolan, W. N. Hardy, R. Kadono, J. R. Kempton, R. F. Kiefl, S. R. Kretzmann, P. Mulhern, T. M. Riseman *et al.*, *Universal Correlations between T_c and n_s/m^* in High- T_c Cuprate Superconductors*, Phys. Rev. Lett. **62**, 2317 (1989), doi:10.1103/PhysRevLett.62.2317.
- [10] I. Hetel, T. R. Lemberger and M. Randeria, *Quantum critical behaviour in the superfluid density of strongly underdoped ultrathin copper oxide films*, Nat. Phys. **3**(10), 700 (2007).
- [11] V. J. Emery and S. A. Kivelson, *Importance of phase fluctuations in superconductors with small superfluid density*, Nature **374**(6521), 434 (1995), doi:10.1038/374434a0.
- [12] J. M. Kosterlitz and D. J. Thouless, *Ordering, metastability and phase transitions in two-dimensional systems*, Jour. Phys. C: Sol. State Phys. **6**(7), 1181 (1973).
- [13] A. Mihlin and A. Auerbach, *Temperature dependence of the order parameter of cuprate superconductors*, Phys. Rev. B **80**(13), 134521 (2009).

- [14] I. Mangel, I. Kapon, N. Blau, K. Golubkov, N. Gavish and A. Keren, *Stiffnessometer: A magnetic-field-free superconducting stiffness meter and its application*, Phys. Rev. B **102**(2), 024502 (2020).
- [15] C. Marin, T. Charvolin, D. Braithwaite and R. Calemczuk, *Properties of a large $La_{1.92}Sr_{0.08}CuO_{4+d}$ single crystal grown by 1.92 0.08 4qd the travelling-solvent floating-zone method*, Physica C **329**, 197 (1999).
- [16] N. Gavish, O. Kenneth and A. Keren, *Ginzburg-Landau model of a stiffnessometer—A superconducting stiffness meter device*, Physica D: Nonlinear Phenomena **415**, 132767 (2021).
- [17] D. J. Scalapino, Y. Imry and P. Pincus, *Generalized Ginzburg-Landau theory of pseudo-one-dimensional systems*, Phys. Rev. B **11**(5), 2042 (1975).
- [18] B. Keimer, A. Aharony, A. Auerbach, R. J. Birgeneau, A. Cassanho, Y. Endoh, R. W. Erwin, M. A. Kastner and G. Shirane, *Néel transition and sublattice magnetization of pure and doped La_2CuO_4* , Phys. Rev. B **45**, 7430 (1992).
- [19] S. T. Bramwell and P. C. W. Holdsworth, *Magnetization: A characteristic of the Kosterlitz-Thouless-Berezinskii transition*, Phys. Rev. B **49**, 8811 (1994), doi:10.1103/PhysRevB.49.8811.
- [20] P. Butera and M. Pernici, *Extended scaling behavior of the spatially anisotropic classical XY model in the crossover from three to two dimensions*, Phys. Rev. B **80**, 054408 (2009), doi:10.1103/PhysRevB.80.054408.
- [21] J. M. Kosterlitz, *The critical properties of the two-dimensional XY model*, Jour. Phys. C: Sol. State Phys. **7**(6), 1046 (1974).
- [22] S. Hikami and T. Tsuneto, *Phase transition of quasi-two dimensional planar system*, Prog. Theor. Phys. **63**(2), 387 (1980).
- [23] S. Hübner, M. Hossain, A. Damascelli and G. Sawatzky, *Two gaps make a high-temperature superconductor?*, Reports on Progress in Physics **71**(6), 062501 (2008).
- [24] W.-S. Lee, I. Vishik, K. Tanaka, D. Lu, T. Sasagawa, N. Nagaosa, T. Devereaux, Z. Hussain and Z.-X. Shen, *Abrupt onset of a second energy gap at the superconducting transition of underdoped $Bi2212$* , Nature **450**(7166), 81 (2007).
- [25] A. Kanigel, U. Chatterjee, M. Randeria, M. Norman, S. Souma, M. Shi, Z. Li, H. Raffy and J. Campuzano, *Protected nodes and the collapse of fermi arcs in high- t c cuprate superconductors*, Physical review letters **99**(15), 157001 (2007).
- [26] S. Teitel and C. Jayaprakash, *Phase transitions in frustrated two-dimensional XY models*, Phys. Rev. B **27**, 598 (1983), doi:10.1103/PhysRevB.27.598.
- [27] U. Wolff, *Collective Monte Carlo Updating for Spin Systems*, Phys. Rev. Lett. **62**, 361 (1989), doi:10.1103/PhysRevLett.62.361.
- [28] A. Del Maestro and I. Affleck, *Interacting bosons in one dimension and the applicability of Luttinger-liquid theory as revealed by path-integral quantum Monte Carlo calculations*, Phys. Rev. B **82**, 060515 (2010), doi:10.1103/PhysRevB.82.060515.
- [29] I. Mangel and A. Keren, *The Ground-state Inter-plane Superconducting Coherence Length of $La_{1.875}Sr_{0.125}CuO_4$ Measured by a "Xiometer"*, arXiv:2308.06757 .

- [30] C. Panagopoulos, J. Cooper, T. Xiang, Y. Wang and C. Chu, *c-axis superfluid response and pseudogap in high- T_c superconductors*, Physical Review B **61**(6), R3808 (2000).
- [31] N. Wada, J. Taniguchi, H. Ikegami, S. Inagaki and Y. Fukushima, *Helium-4 Bose fluids formed in one-dimensional 18 diameter pores*, Phys. Rev. Lett. **86**(19), 4322 (2001).
- [32] R. Toda, M. Hieda, T. Matsushita, N. Wada, J. Taniguchi, H. Ikegami, S. Inagaki and Y. Fukushima, *Superfluidity of He4 in One and Three Dimensions Realized in Nanopores*, Phys. Rev. Lett. **99**(25), 255301 (2007).
- [33] D. F. Agterberg, J. S. Davis, S. D. Edkins, E. Fradkin, D. J. Van Harlingen, S. A. Kivelson, P. A. Lee, L. Radzihovsky, J. M. Tranquada and Y. Wang, *The physics of pair-density waves: Cuprate superconductors and beyond*, Annual Review of Condensed Matter Physics **11**(1), 231 (2020), doi:10.1146/annurev-conmatphys-031119-050711, <https://doi.org/10.1146/annurev-conmatphys-031119-050711>.
- [34] Y.-H. Li and S. Teitel, *Finite-size scaling study of the three-dimensional classical XY model*, Phys. Rev. B **40**, 9122 (1989).
- [35] F. Hrahsheh and T. Vojta, *Anomalous elasticity in a disordered layered XY model*, Phys. Scripta **2012**(T151), 014074 (2012).
- [36] A. W. Sandvik, *Computational studies of quantum spin systems*, In *AIP Conference Proceedings*, vol. 1297, pp. 135–338. American Institute of Physics (2010).